Bull. Mater. Sci., Vol. 40, No. 6, October 2017, pp. 1075–1080
DOI 10.1007/s12034-017-1483-0

Synthesis and up-conversion emissions of Yb^{3+}/Er^{3+}, Yb^{3+}/Tm^{3+} and $Yb^{3+}/Tm^{3+}/Gd^{3+}$ co-doped KLu_2F_7

CHUNYAN CAO[1,2,*], AN XIE[1,2], HYEON MI NOH[3] and JUNG HYUN JEONG[3]
[1]School of Materials Science and Engineering, Xiamen University of Technology, Xiamen 361024, China
[2]Key Laboratory of Functional Materials and Applications of Fujian Province, Xiamen 361024, China
[3]Department of Physics, Pukyong National University, Busan 608-737, Korea
*Author for correspondence (caoyan_80@xmut.edu.cn)

MS received 17 September 2016; accepted 1 March 2017; published online 23 September 2017

Abstract. Yb^{3+}/Er^{3+}, Yb^{3+}/Tm^{3+}, or $Yb^{3+}/Tm^{3+}/Gd^{3+}$ co-doped KLu_2F_7 up-conversion (UC) materials were synthesized through a hydrothermal method or an additive-assisted hydrothermal method. The X-ray diffraction (XRD) results suggested that the materials crystallized in orthorhombic phase, yet, the potassium citrate (CitK) introduction affected immensely the crystalline purity of final material. The field emission scanning electron microscopy (FE-SEM) results suggested that the additive adding had effects on size and morphology of the material, which affected the UC emissions further. Green/red UC emissions of Er^{3+}, UV/blue/IR UC emissions of Tm^{3+}, and UV UC emissions of Gd^{3+} were observed in the orthorhombic phase of KLu_2F_7 materials. The excitation power-dependent UC emissions illustrated that the UC emission intensity initially increased, then decreased with the increase in excitation power. At the same time, the variation rates of different transitions in Er^{3+} or Tm^{3+} are also different. In addition, the Er^{3+} or Tm^{3+} concentration-dependent UC emission results suggested that the optimal doping concentration of Er^{3+} is 2 mol% and Tm^{3+} is 0.5 mol% with the Yb^{3+} concentration fixed as 20 mol%. The experimental results suggest that the orthorhombic phase of KLu_2F_7 should be a good host lattice for UC emitters.

Keywords. Hydrothermal synthesis; up-conversion; optical properties; rare earth.

1. Introduction

In the last few decades, rare earth (RE) materials have been extensively studied because of their potential applications in high performance magnets, luminescent devices, catalysts and other functional materials based on 4f electrons in RE^{3+} [1–5]. Rare earth fluorides, which possess high refractive indexes and low phonon energies, have attracted more attention especially for up-conversion (UC) emission research [6–10]. UC emission is one of the physical processes to change the frequency of light through multistep absorptions, energy transfers (ETs), cross relaxation (CR), excited state absorption (ESA) processes [11], etc. UC host lattice materials, such as $NaYF_4$ and $NaGdF_4$, have been widely studied because of their potential applications in optical data storage, colour displays, IR sensors, environmental monitoring, biosensors [12,13], etc. Recently, there are some reports on the $NaLuF_4$ host materials, which are also expected to be excellent host material for UC emissions [14–17], such as Yb^{3+}/Tm^{3+}, Yb^{3+}/Tm^{3+}, Yb^{3+}/Ho^{3+}, etc. The Lu^{3+}may be more favourable than that of usually used Y^{3+} as host ions for the Lu^{3+} doping can remarkably tune the luminescent properties [18,19].

Material scientists have explored various synthetic strategies for the synthesis of materials in the past 10 years. Dramatic efforts have been dedicated to synthesize RE fluoride nano-/micro-crystals with uniform size and shape, such as hydrothermal synthesis [20,21], rotary evaporator method [10], thermal decomposition route [22], etc. The hydrothermal treatment method has been proved to be effective and convenient in preparing various inorganic materials with diverse controllable morphologies and architectures [23,24]. Especially, the hydrothermal method is simple, mild and easy to produce a large amount of products. Therefore, in the present study, the hydrothermal method is adopted to synthesize fluoride materials.

In fluoride material series, there is another important alkali RE-based fluoride, $KREF_4$, which has received considerable attention for material studies [25–28]. Yet, there is less attention for the synthesis and UC emission studies of KLu_2F_7 microcrystals, which is also should be a good host material for UC emission emitters. By using a hydrothermal method or a surfactant-assisted hydrothermal method, and adjusting the introduction concentration of Er^{3+}, Tm^{3+}, Gd^{3+}, 20 mol% Yb^{3+} and the above RE^{3+} co-doped KLu_2F_7 microcrystals were synthesized. The final products that were crystallized in the orthorhombic phase, and the material particles are in micrometre size with the hexagonal disk or flower-like morphologies composed of crashed hexagonal disks. With a 980 nm laser diode (LD) excitation, the UC emission of

Er^{3+}, Tm^{3+} and Gd^{3+} were recorded. Though, the energy gap between the ground state $^8S_{7/2}$ and the first excited state $^6P_{7/2}$ of Gd^{3+} is about 32,000 cm^{-1} (~313 nm), the UV UC emissions of Gd^{3+} were recorded in $Yb^{3+}/Tm^{3+}/Gd^{3+}$ co-doped KLu_2F_7 microcrystals. The Er^{3+}, Tm^{3+} concentrations and excitation power-dependent UC emissions were also studied.

2. Experimental

The materials were synthesized through a hydrothermal method or an additive-assisted hydrothermal method. The raw materials, Lu_2O_3 (4N), Yb_2O_3 (4N), Er_2O_3 (4N), Tm_2O_3 (4N) and Gd_2O_3 (4N) were all purchased from Shanghai Yuelong New Materials Co. Ltd., China. The dehydrated KF (99.5%), polyethylene glycol 10000 (PEG 10000), polyvinylpyrrolidone K30 (PVP K30) and $K_3C_6H_5O_7 \cdot H_2O$ (CitK A.R.) were purchased from Sinopharm Chemical Reagent Co. Ltd., China. Polyetherimide (PEI) (50% in water) was purchased from Aldrich Sigma. The materials were synthesized in a similar procedure as mentioned in ref. [28], except the corresponding raw materials were replaced. Some additives, such as PEG, PEI, PVP and potassium citrate (CitK) were also added in the preparation procedure of some samples to control the morphology and optical properties of the materials.

To identify the crystallization phases, X-ray diffraction (XRD) analysis was performed on an X'pert diffractometer with CuKα ($\lambda = 1.5406$ Å) radiation at 40 kV and 40 mA. A Hitachi SU8020 field emission scanning electron microscopy (FE-SEM) was used to characterize the morphologies and sizes of some obtained materials. Under a 980 nm LD excitation, UC emission spectra of the obtained materials were recorded with a fluorescence spectrophotometer (Hitachi F-7000).

3. Results and discussion

Figure 1 illustrates some representative XRD patterns of samples and reference data. The XRD pattern (figure 1a) of the 20 mol% Yb^{3+}, 2 mol% Er^{3+} co-doped sample synthesized without additive-adding can be indexed to the orthorhombic phase of KYb_2F_7 with JCPDS 27-0459. The results suggest that the sample is isostructural to that of the orthorhombic phase of KYb_2F_7 and can be named as orthorhombic phase of KLu_2F_7. No impurity lines were observed in the pattern, meaning that the Yb^{3+}/Er^{3+} doping does not cause significant change in the samples. Additives PEG (5 wt.%) (figure 1b), PVP (5 wt.%) (figure 1c), and PEI (5 wt.%) (figure 1d) were added in the synthesis procedure, the samples kept the orthorhombic phase besides the diffraction peak intensity variations. Yet, when 2 molar ratio of CitK was added to that of RE^{3+} in the synthesis procedure, the XRD pattern (figure 1e) of obtained sample had new peaks (marked as *), suggesting that the CitK adding resulted in new crystalline phase. The CitK adding introduced the K^+ and the pH value of prepared solution measured by pH test paper varied from about 6.5 to 3.3 with the CitK adding. With reference to the molar ratio of raw material and the pH value of prepared solution-dependent materials [20,21], the new crystalline phase is formed by the introduction of additive K^+ and the variation of pH value in the prepared solution.

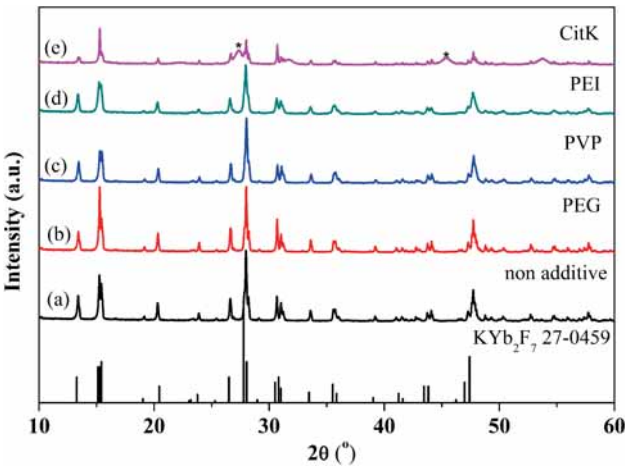

Figure 1. XRD patterns of Yb^{3+}/Er^{3+} co-doped some samples with (**a**) non-additive, (**b**) PEG, (**c**) PVP, (**d**) PEI and (**e**) CitK adding.

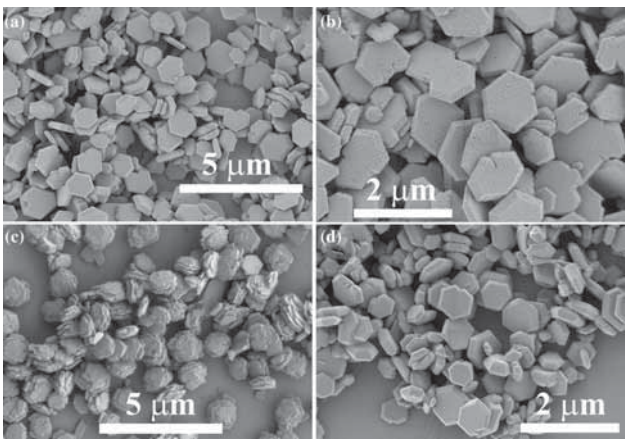

Figure 2. FE-SEM images of Yb^{3+}/Er^{3+} co-doped KLu_2F_7: (**a**) non-additive, (**b**) PEG, (**c**) PEI and (**d**) PVP.

The FE-SEM images of some selected samples are illustrated in figure 2. The non-additive-added KLu_2F_7 sample presents hexagonal disk morphology with an average edge size of about 1 μm, as presented in figure 2a. The PEG adding has no great effects on the morphology, and the average size of the hexagonal disk became smaller which is about 700 nm, as shown in figure 2b. Figure 2c illustrated the FE-SEM micrograph of the sample with PEI adding. The sample was composed of micro flower-like particles which were assemblies of crashed hexagonal disks with average size of about 300 nm. The FE-SEM picture suggests that the PEI adding has great effects on the morphologies and sizes of the final samples. The PVP adding has no great effects on the

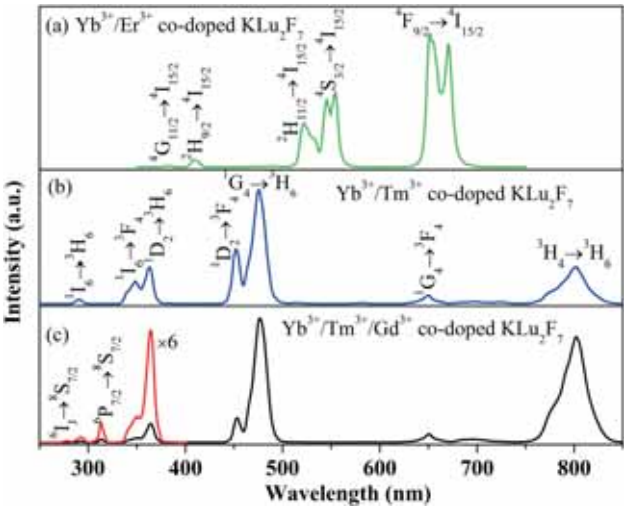

Figure 3. Up-conversion emission of (**a**) Yb^{3+}/Er^{3+}, (**b**) Yb^{3+}/Tm^{3+} and (**c**) $Yb^{3+}/Tm^{3+}/Gd^{3+}$ co-doped KLu_2F_7.

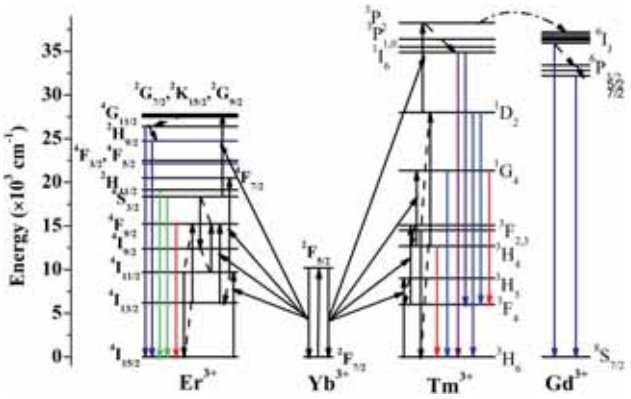

Figure 4. Energy level diagrams of Yb^{3+}, Er^{3+}, Tm^{3+} and Gd^{3+}, and possible up-conersion processes.

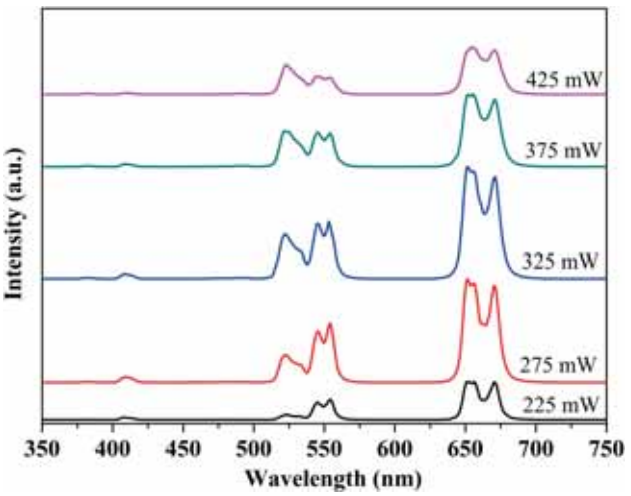

Figure 5. Excitation power-dependent UC emission spectra of Yb^{3+}/Er^{3+} co-doped KLu_2F_7.

morphology of the final sample (figure 2d), yet, the additive affected the average size of the microparticles which have an average edge size of about 500 nm. The morphologies and the average sizes of the samples would affect the optical properties further.

UC emission spectra of 20 mol% Yb^{3+}, 2 mol% Er^{3+}, 20 mol% Yb^{3+}, 0.5 mol% Tm^{3+}, and 20 mol% Yb^{3+}, 0.5 mol% Tm^{3+} and 3 mol% Gd^{3+} co-doped KLu_2F_7 are shown in figure 3a–c, respectively. In the samples, 20 mol% Yb^{3+}, 2 mol% Er^{3+} co-doped KLu_2F_7, with a 980 nm LD radiation, strong green emissions peaked at 522 and 554 nm originated from Er^{3+} transitions of $^2H_{11/2} \rightarrow {}^4I_{15/2}$ and $^4S_{3/2} \rightarrow {}^4I_{15/2}$, respectively. Strong red emission peaked at 651 nm can be ascribed to the transition of $^4F_{9/2} \rightarrow {}^4I_{15/2}$ of Er^{3+}. In addition, weak emissions located at 382 and 408 nm were also recorded, which were Er^{3+} transitions of $^4G_{11/2} \rightarrow {}^4I_{15/2}$ and $^2H_{9/2} \rightarrow {}^4I_{15/2}$, respectively. UC emission spectra of 20 mol% Yb^{3+} and 0.5 mol% Tm^{3+} co-doped KLu_2F_7 from UV to IR range are shown in figure 3b. Strong blue UC emission peaked at 476 nm and IR UC located at 802 nm originate from the Tm^{3+} transition of $^1G_4 \rightarrow {}^3H_6$ and $^3H_4 \rightarrow {}^3H_6$, respectively. UV UC emission peaked at 290, 350 and 365 nm are Tm^{3+} transitions of $^1I_6 \rightarrow {}^3H_6$, $^1I_6 \rightarrow {}^3F_4$ and $^1D_2 \rightarrow {}^3H_6$, respectively. In addition, violet UC emission peaked at 452 nm and weak red emission peaked at 650 nm can be ascribed to Tm^{3+} transitions of $^1D_2 \rightarrow {}^3F_4$ and $^1G_4 \rightarrow {}^3F_4$, respectively. Compared to the Yb^{3+}/Tm^{3+} co-doped KLu_2F_7, there are UV UC emissions of Gd^{3+} in addition to the UC emissions of Tm^{3+} in the $Yb^{3+}/Tm^{3+}/Gd^{3+}$ co-doped KLu_2F_7. For clarity, the UV UC emission in the wavelength range of 250–400 nm was magnified six times for the intensity that was weak. The emission that centred at 277 nm comes from $^6I_J \rightarrow {}^8S_{7/2}$ transitions of Gd^{3+}. And the emission peaked at 313 nm originate from $^6P_{7/2} \rightarrow {}^8S_{7/2}$ transition of Gd^{3+}. For clarity, the energy level diagrams of Yb^{3+}, Er^{3+}, Tm^{3+} and Gd^{3+}, and possible UC processes are schematically plotted in figure 4. According to UC mechanism [11], past work [29–32] and present data, the UC emissions of Er^{3+}, Tm^{3+} or Gd^{3+} were caused by ET, CR, ESA, etc. processes in Yb^{3+}, Er^{3+}, Tm^{3+}, or Gd^{3+} ions. The above UC spectra suggested that the KLu_2F_7 is a good host lattice for UC emission ions, such as Er^{3+}, Tm^{3+}, Gd^{3+}, etc.

It is well known that excitation power has great effects on the emission intensities. Figure 5 shows the excitation power-dependent UC emission spectra of sample 20 mol% Yb^{3+}, 2 mol% Er^{3+} co-doped KLu_2F_7. With the excitation power of the 980 nm LD increasing, the emission intensity initially increased and then decreased. The variation rates of the $^2H_{11/2} \rightarrow {}^4I_{15/2}$ and $^4S_{3/2} \rightarrow {}^4I_{15/2}$ were different, the intensity ratio of $^2H_{11/2} \rightarrow {}^4I_{15/2}$ (peaked at 522 nm) to $^4S_{3/2} \rightarrow {}^4I_{15/2}$ (peaked at 554 nm) increased with the increase in excitation power, which was caused by thermal relaxation process and can be used in temperature sensors. Figure 6 illustrates the variations clearly.

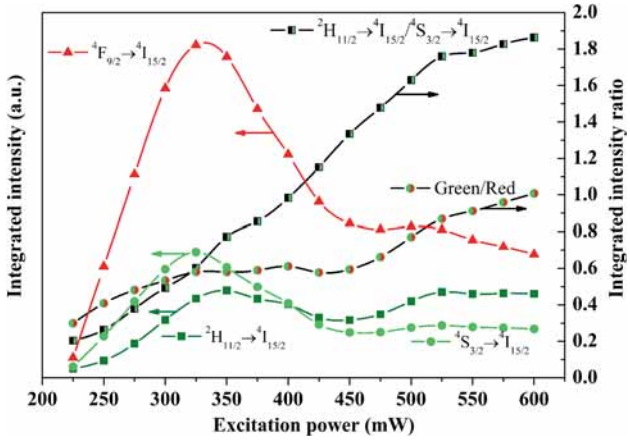

Figure 6. Integrated emission intensity of $^2H_{11/2} \rightarrow{}^4I_{15/2}$, $^4S_{3/2} \rightarrow{}^4I_{15/2}$, $^4F_{9/2} \rightarrow{}^4I_{15/2}$ and integrated emission intensity ratio of $^2H_{11/2} \rightarrow{}^4I_{15/2}/^4S_{3/2} \rightarrow{}^4I_{15/2}$, green/red emissions dependent on excitation power in Yb^{3+}/Er^{3+} co-doped KLu_2F_7.

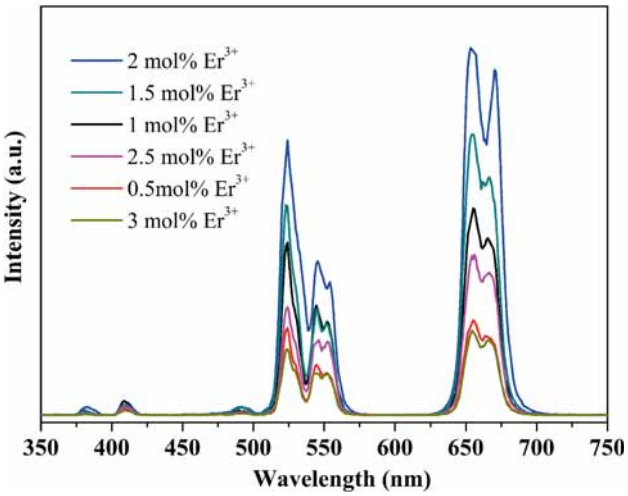

Figure 7. Up-conversion emission spectra of 20 mol% Yb^{3+}, x mol% Er^{3+} co-doped KLu_2F_7.

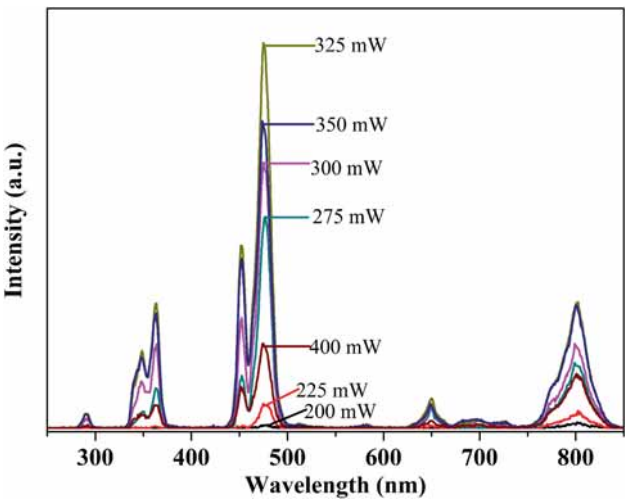

Figure 8. Excitation power-dependent UC emission spectra of Yb^{3+}/Tm^{3+} co-doped KLu_2F_7.

With the increase in excitation power, the emission intensity initially increased and then decreased. Figure 6 shows the integrated emission intensities of $^2H_{11/2} \rightarrow{}^4I_{15/2}$, $^4S_{3/2} \rightarrow{}^4I_{15/2}$, $^4F_{9/2} \rightarrow{}^4I_{15/2}$, and integrated emission intensity ratios of $^2H_{11/2} \rightarrow{}^4I_{15/2}/^4S_{3/2} \rightarrow{}^4I_{15/2}$ and green/red emissions dependent on excitation power in 20 mol% Yb^{3+}, 2 mol% Er^{3+} co-doped KLu_2F_7. As shown in figure 6, the green and the red emission intensities initially increased quickly with the increase in excitation power. When the excitation power is about 325 mW, the green and red emissions reached the maxima. With the increase in excitation power further, the red $^4F_{9/2} \rightarrow{}^4I_{15/2}$ emission decreased rapidly and completely. The green $^4S_{3/2} \rightarrow{}^4I_{15/2}$ emission decreased rapidly and then slightly increased, and remained unvaried. The green $^2H_{11/2} \rightarrow{}^4I_{15/2}$ emission also decreased rapidly and then increased and almost remained unvaried. The variation rates of the two green emissions are different. To investigate the emission intensity dependence on excitation power in detail, the green emission intensity ratios of $^2H_{11/2} \rightarrow{}^4I_{15/2}/^4S_{3/2} \rightarrow{}^4I_{15/2}$ and the green/red rate *vs.* the excitation power are also plotted in figure 6, where the green emission includes the emissions of $^2H_{11/2} \rightarrow{}^4I_{15/2}$ and $^4S_{3/2} \rightarrow{}^4I_{15/2}$. The emission ratio of $^2H_{11/2} \rightarrow{}^4I_{15/2}$ to $^4S_{3/2} \rightarrow{}^4I_{15/2}$ always increased with the increasing excitation power, which was caused by thermal relaxation. The ratio of green to red emissions increased with the increasing excitation power, suggesting that the variation rates of green and red emissions are different.

In addition, Er^{3+} concentration-dependent UC emissions were also investigated. Figure 7 shows the UC emission spectra of 20 mol% Yb^{3+}, x mol% Er^{3+} co-doped KLu_2F_7, which were recorded under the same measurement conditions. Once the Yb^{3+} concentration is fixed at 20 mol%, the UC emission intensity is initially increased, and reached the maximum when the Er^{3+} concentration was 2 mol%, then decreased with the increase in Er^{3+} concentration further. The results suggested that the doping concentration has great effects on the UC emission intensity and the optimum concentration of Er^{3+} is 2 mol% in this case.

With the increase in excitation power, the UC emission spectra of 20 mol% Yb^{3+}, 0.5 mol% Tm^{3+} co-doped KLu_2F_7 are illustrated in figure 8. When the excitation power is low, only IR and blue UC emissions were recorded, with the increase in excitation power, the UV UC emissions emerged and became stronger. The UC emission intensities reached the maxima when the excitation power is about 325 mW, then became weaker with the increase in excitation power further. As shown in figure 8, the blue and UV UC emissions decreased rapidly than that of IR UC emissions.

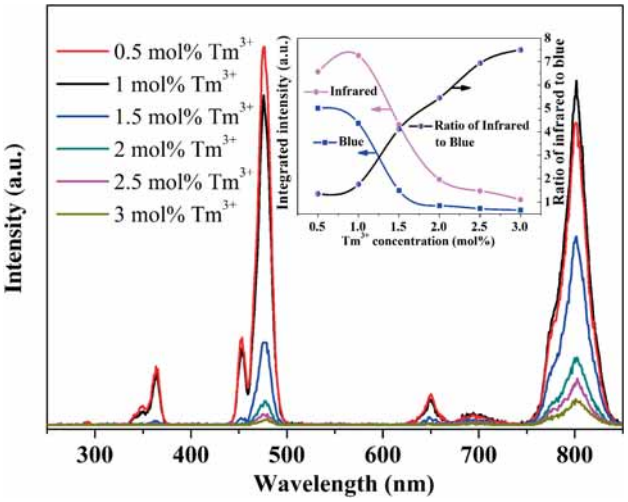

Figure 9. Up-conversion emission spectra of 20 mol% Yb^{3+}, y mol% Tm^{3+} co-doped KLu_2F_7. Inset shows integrated intensity of blue and infrared emissions, and ratio of infrared to blue.

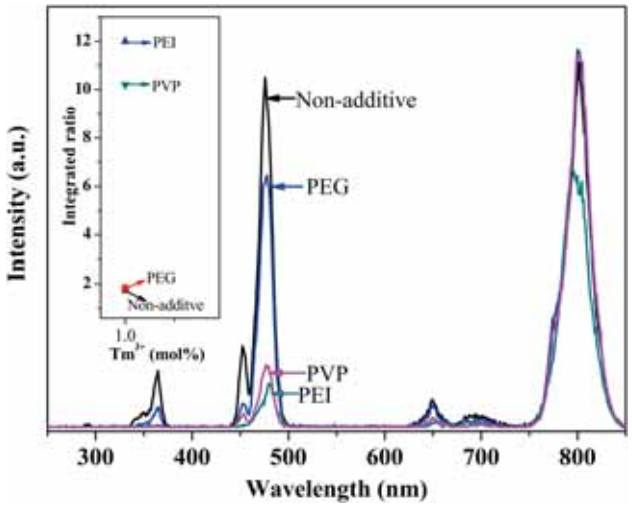

Figure 10. UC emission spectra of non-additive-assisted hydrothermal synthesized 20 mol% Yb^{3+}, 1 mol% Tm^{3+} co-doped KLu_2F_7. Inset shows the integrated up-conversion intensity ratio of infrared to blue.

Similarly, Tm^{3+} concentration-dependent UC emission spectra are also investigated as shown in figure 9. Under the same measurement conditions, the Yb^{3+} concentration is fixed at 20 mol%, the UC emission intensity decreased with the increase in Tm^{3+} concentration. Similar to the excitation power-dependent UC emission intensity, the Tm^{3+} concentration also has great effects on the UC emission intensities, as shown in the inset of figure 9. With the increase in Tm^{3+} concentration, the integrated blue UC emission (from 435 to 505 nm) intensity decreased, while the IR UC emission (in the range of 745–850 nm) intensity initially increased, and then decreased. The decrease rates of the blue and IR UC emissions were different. The integrated ratio of IR to blue increased always, which suggested that the blue UC emission decreased rapidly than that of infrared UC emissions. The relatively high concentration of Tm^{3+} is not good for UV and blue UC emissions.

In addition, the UC emission spectra of additive-assisted and non-additive-assisted hydrothermal synthesized 20 mol% Yb^{3+}, 1 mol% Tm^{3+} co-doped KLu_2F_7 were compared and studied. As illustrated in figure 10, the non-additive-assisted hydrothermal synthesized 20 mol% Yb^{3+}, 1 mol% Tm^{3+} co-doped KLu_2F_7 presents the strongest UV and blue UC emissions. The PVP- and PEI-assisted hydrothermal synthesized samples have almost no UV UC emissions. The additive-assisted hydrothermal synthesized Yb^{3+}/Tm^{3+} co-doped KLu_2F_7 has strong IR UC emissions than that of blue UC emissions. The integrated intensity ratio of IR UC emission to that of blue UC emission is shown in the inset of figure 10. The PEG-assisted and non-additive assisted hydrothermal synthesized Yb^{3+}/Tm^{3+} co-doped KLu_2F_7 presents low ratio of IR to blue UC emission. On the contrary, the PEI- and PVP-assisted hydrothermal synthesized samples illustrate the high ratio of IR to blue UC emission. The strong IR UC emission is good for the biological applications of the samples.

4. Conclusions

In conclusion, through a hydrothermal method or an additive-assisted hydrothermal method, Yb^{3+}/Er^{3+}, Yb^{3+}/Tm^{3+} and $Yb^{3+}/Tm^{3+}/Gd^{3+}$ co-doped KLu_2F_7 materials are synthesized. The XRD results suggested that the KLu_2F_7 crystallized in orthorhombic phase, yet, the CiK adding affect the crystalline purity. The FE-SEM results suggested that the material particle in micrometre size and the additive adding have effects on the morphology of particles, which affected the UC emissions further. The excitation power-dependent UC emission spectra suggested that the UC emission intensity initially increased, then decreased with the increase in excitation power, while the variations of UC transitions in Er^{3+} or Tm^{3+} are different. With the Yb^{3+} concentration fixed at 20 mol%, the Er^{3+} or Tm^{3+} concentration-dependent UC emission spectra suggested that the optimal doping concentration of Er^{3+} is 2 mol% and Tm^{3+} is 0.5 mol% in this case. The results suggested that the KLu_2F_7 is a good host material for UC emitters and has potential applications in biology.

Acknowledgements

This work was financially supported by National Natural Science Foundation of China (grant nos. 61205217 and 11204258), Natural Science Foundation of Fujian Province (grant no. 2017J01719), Program for New Century Excellent

Talents in University of Fujian Province for 2015 and 2014 (grant no. ZA14228), Project of Science and Technology Plan of Fujian Province (grant no. 2016H0037), Science and Technology Plan of Xiamen City (grant nos. 3502Z20151236 and 3502Z20153018). This research was also supported by Basic Science Research Program through the National Research Foundation of Korea (NRF), funded by the Ministry of Science, ICT and Future Planning (grant no. 2015060315). Some samples were supplied by the Display and Lighting Phosphor Bank at Pukyong National University.

References

[1] Yang D M, Ma P A, Hou Z Y, Cheng Z Y, Li C X and Lin J 2015 *Chem. Soc. Rev.* **44** 1416
[2] Chen K-H, Weng M-H, Yang R-Y and Pan C-T 2016 *Bull. Mater. Sci.* **39** 1171
[3] Palan C B, Bajaj N S, Soni A and Omanwar S K 2016 *Bull. Mater. Sci.* **39** 1157
[4] Keshavamurthy K and Eraiah B 2015 *Bull. Mater. Sci.* **38** 1381
[5] Li C X and Lin J 2010 *J. Mater. Chem.* **20** 6831
[6] Tu D, Liu L, Ju Q, Liu Y, Zhu H, Li R *et al* 2011 *Angew. Chem. Int. Ed.* **50** 6306
[7] Wang Z H, Hao J H, Chan H L W, Law G-L, Wong W-T *et al* 2011 *Nanoscale* **3** 2175
[8] Cao C Y, Xie A, Noh H M and Jeong J H 2016 *Luminescence* **31** 1063
[9] Wang F, Han Y, Lim C S, Lu Y, Wang J *et al* 2010 *Nature* **463** 1061
[10] Ju Q, Tu D, Liu Y, Li R, Zhu H *et al* 2012 *J. Am. Chem. Soc.* **134** 1323
[11] Auzel F 2004 *Chem. Rev.* **104** 139
[12] Zhang F, Shi Q, Zhang Y, Shi Y, Ding K *et al* 2011 *Adv. Mater.* **23** 3775
[13] Zheng W, Huang P, Tu D, Ma E, Zhu H and Chen X 2015 *Chem. Soc. Rev.* **44** 1379
[14] Liu Q, Sun Y, Yang T S, Feng W, Li C G *et al* 2011 *J. Am. Chem. Soc.* **133** 17122
[15] Yang T, Sun Y, Liu Q, Feng W, Yang P *et al* 2012 *Biomaterials* **33** 3733
[16] Shi F, Wang J S, Zhai X S, Zhao D and Qin W P 2011 *CrystEngComm.* **13** 3782
[17] Zhu W, Zhao S L, Liang Z Q, Yang Y X, Zhang J J *et al* 2016 *J. Alloys Compd.* **659** 146
[18] Capobianco J A, Vetrone F, Boyer J C, Speghini A and Bettinelli M 2002 *Opt. Mater.* **19** 259
[19] Xia A, Chen M, Gao Y, Wu D M, Feng W, Li F Y *et al* 2012 *Biomaterials* **33** 5394
[20] Cao C Y, Yang H K, Chung J W, Moon B K, Choi B C *et al* 2011 *J. Mater. Res.* **26** 2916
[21] Cao C Y, Yang H K, Chung J W, Moon B K, Choi B C *et al* 2011 *Opt. Commun.* **284** 5453
[22] Zhang Y, Sun X, Si R, You L and Yan C 2005 *J. Am. Chem. Soc.* **127** 3260
[23] Liang J H, Peng Q, Wang X, Zheng X, Wang R J *et al* 2005 *Inorg. Chem.* **44** 9405
[24] Ladol J, Khajuria H, Khajuria S and Sheikh H N 2016 *Bull. Mater. Sci.* **39** 943
[25] Yang L W, Zhang Y Y, Li J J, Li Y, Zhong J X *et al* 2010 *Nanoscale* **2** 2805
[26] Wong H-T, Vetrone F, Naccache R, Chan H L W, Hao J H *et al* 2011 *J. Mater. Chem.* **21** 16589
[27] Schäfer H, Ptacek P, Zerzouf O and Haase M 2008 *Adv. Funct. Mater.* **18** 2913
[28] Cao C Y, Yang H K, Chung J W, Moon B K, Choi B C *et al* 2011 *J. Mater. Chem.* **21** 10342
[29] Cao C Y, Qin W P, Zhang J S, Wang Y, Zhu P F *et al* 2008 *Opt. Lett.* **33** 857
[30] Qin W P, Cao C Y, Wang L L, Zhang J S, Zhang D S *et al* 2008 *Opt. Lett.* **33** 2167
[31] Cao C Y, Zhang X M, Chen M L, Qin W P and Zhang J S 2010 *J. Alloys Compd.* **505** 6
[32] Zheng K Z, Qin W P, Cao C Y, Zhao D and Wang L L 2015 *J. Phys. Chem. Lett.* **6** 556